HHS Public Access

Author manuscript

Arterioscler Thromb Vasc Biol. Author manuscript; available in PMC 2023 January 01.

Published in final edited form as:

Arterioscler Thromb Vasc Biol. 2022 January ; 42(1): 6–18. doi:10.1161/ATVBAHA.120.315501.

Loss of Id3 increases the number of IgM-producing B-1b cells in ischemic skeletal muscle impairing blood flow recovery during hind limb ischemia

Victoria Osinski[1,2], **Prasad Srikakulapu**[3], **Young Min Haider**[3], **Melissa A. Marshall**[3], **Vijay C. Ganta**[4], **Brian H. Annex**[4,5], **Coleen A. McNamara**[1,3,6]

[1]Robert M. Berne Cardiovascular Research Center, University of Virginia, Charlottesville, Virginia 22908

[2]Department of Pathology, University of Virginia, Charlottesville, Virginia 22908

[3]Beirne B. Carter Center for Immunology Research, University of Virginia, Charlottesville, Virginia 22908

[4]Vascular Biology Center, Augusta University, Augusta, Georgia 30912

[5]Department of Medicine, Medical College of Georgia, Augusta University, Augusta, Georgia 30912

[6]Department of Medicine, Division of Cardiovascular Medicine, University of Virginia, Charlottesville, Virginia 22908

Abstract

Objective: Neovascularization can maintain and even improve tissue perfusion in the setting of limb ischemia during peripheral artery disease (PAD). The molecular and cellular mechanisms mediating this process are incompletely understood. We investigate the potential role(s) for Inhibitor of differentiation 3 (Id3) in regulating blood flow in a murine model of hind limb ischemia (HLI).

Approach and Results: HLI was modeled through femoral artery ligation and resection and blood flow recovery was quantified by Laser Doppler perfusion imaging. Mice with global Id3 deletion had significantly impaired perfusion recovery at 14 and 21 days of HLI. Endothelial- or myeloid cell-specific deletion of Id3 revealed no effect on perfusion recovery while B cell-specific knockout of Id3 ($Id3^{BKO}$) revealed a significant attenuation of perfusion recovery. Flow cytometry revealed no differences in ischemia-induced T cells or myeloid cell numbers at 7 days of HLI, yet there was a significant increase in B-1b cells in $Id3^{BKO}$. Consistent with these findings, ELISA

Corresponding Author: Coleen A. McNamara, Address: 345 Crispell Dr, MR-6, RM #3520, Charlottesville, VA 22908, cam8c@virginia.edu, Telephone: 434-243-5854.

Disclosures

The authors report no conflicts of interests.

Supplemental Materials

Expanded Materials & Methods

Online Figures S1–S14

Online Tables S1–S6

demonstrated increases in skeletal muscle and plasma IgM. *In vitro* experiments demonstrated reduced proliferation and increased cell death when ECs were treated with conditioned media from IgM-producing B-1b cells and tibialis anterior muscles in $Id3^{BKO}$ mice showed reduced density of total $CD31^+$ and αSMA^+CD31^+ vessels.

Conclusions: This study is the first to demonstrate a role for B cell-specific Id3 in maintaining blood flow recovery during HLI. Results suggest a role for Id3 in promoting blood flow during HLI and limiting IgM-expressing B-1b cell expansion. These findings present new mechanisms to investigate in PAD pathogenesis.

Keywords

ischemia; B cells; Id3; neovascularization; IgM

Subject Terms:

Ischemia; Inflammation; Angiogenesis

Introduction:

Peripheral artery disease (PAD) is a prevalent vascular disease with many co-morbidities and few effective therapeutic options[1–3]. There is a need to identify novel molecular and cellular mechanisms regulating the capacity for individuals to maintain adequate tissue vascularization in response to reduced blood flow in major peripheral arteries. This can occur through arteriogenesis and/or angiogenesis[4] mediated by many different factors including genetics, lifestyle, lipid levels and inflammation[1,5,6]. In this study, we investigated the potential role(s) for the transcription factor Inhibitor of differentiation 3 (Id3) in regulating vascularization during skeletal muscle ischemia.

Id3 is a broadly expressed member of the helix-loop-helix transcription factor family that regulates cell proliferation, differentiation, and responses to hyperlipidemia and cytokines including growth factors and inflammatory stimuli[7–12]. Our lab has previously identified a single nuclear polymorphism (SNP) in the coding region of the human *ID3* gene. Expression of the minor allele of this SNP results in an amino acid change which attenuates binding with its partner protein E12. The minor allele also correlates with worsened indices of atherosclerosis[13,14]. Loss of Id3 in mice attenuates neovascularization during tumor growth and adipose tissue expansion[15,16]. Additional studies demonstrated that loss of expression of both Id3 and Id1, another HLH transcription factor with overlapping functions, attenuated muscle recovery during skeletal muscle ischemia[17] and reduces capillary density during ischemic renal injury[18]. These studies, however, did not assess the individual role of Id3 on neovascularization. Thus, whether loss of Id3 alone impairs perfusion recovery in response to hind limb ischemia (HLI) remains unknown.

Importantly, Id3 plays a major role in lymphocyte biology, particularly in their growth and development[19]. Loss of Id3 has been shown to alter B lymphocyte trafficking to blood vessels[20]. B cells are primarily divided into innate B-1 cells and adaptive or conventional B-2 cells. B-1 cells produce Natural antibodies, predominantly of the IgM isotype. B-1

cells can be subdivided into B-1a and B-1b subtypes based on their expression of CD5[21,22]. Notably, B cell-specific deletion of Id3 increased the number of B-1b cells in spleen, peritoneal cavity and blood[23].

The immune system and inflammation have an established role in regulating blood flow and neovascularization in the setting of ischemia, though very little is known about the role that B cells, and specifically B-1 cells, may play in this process. Prior cell-specific knockout studies have demonstrated essential roles for endothelial cells (ECs)[24,25] and macrophages[26–30] in regulating ischemic neovascular adaptation in skeletal muscle. A recent study also demonstrated a role for Id3 in regulating endothelial function and proliferation in the bone marrow[31]. To our knowledge, however, no studies of B-1b cells in angiogenesis or perfusion recovery after HLI exist. Together, this provides rationale for investigating the roles of global and cell-specific Id3 expression in a murine model of hind limb ischemia (HLI).

Materials & Methods

The data that support the findings of this study are available from the corresponding author upon reasonable request.

Reagents

Buffers and other solutions prepared for experiments are described in Table S1. Antibodies were purchased from Biolegend, BD Biosciences, Sigma Aldrich, ThermoFisher, eBiosciences, Miltenyi, Dianova, SouthernBiotech as specified in Tables S2–4. Primers were designed in-house and synthesized by IDT.

Mice

Knockout mice on a C57BL/6J background were generated and housed at the University of Virginia. All animal experiments performed in this study were approved by the Institutional Animal Care and Use Committee of the University of Virginia.

Genetic knockout models—Five transgenic knockout lines were maintained and utilized in these studies: Id3 global knockout (KO) and wild type (WT) littermates ($Id3^{GWT}$ and $Id3^{GKO}$, respectively), Id3 B cell-specific KO and WT littermates ($Id3^{fl/fl}CD19^{cre/+}$ ($Id3^{BKO}$) and $Id3^{fl/fl}CD19^{+/+}$ ($Id3^{BWT}$)), Id3 myeloid-specific KO and WT littermates ($Id3^{fl/fl}Lysm^{cre/+}$ ($Id3^{MKO}$) and $Id3^{fl/fl}Lysm^{+/+}$ ($Id3^{MWT}$)), Id3 EC-specific conditional KO and WT littermates ($Id3^{fl/fl}$Cdh5-CreER^{T2} ($Id3^{ECKO}$) and $Id3^{+/+}$Cdh5-Cre/ER^{T2} ($Id3^{ECWT}$)), and secreted IgM deficient and WT littermates ($sIgM^{-/-}$ and $sIgM^{+/+}$). To induce Id3 KO in the conditional knockout line, $Id3^{ECKO}$ and $Id3^{ECWT}$ mice were administered 1 mg of tamoxifen via intraperitoneal injection per day for ten days over the course of two weeks. Tamoxifen was resuspended in peanut oil at a concentration of 10 mg/mL and filter-sterilized prior to administration. Two weeks were allocated for tamoxifen wash-out following the final injection and prior to the start of any treatments or studies.

Model of hind limb ischemia (HLI)—To induce hind limb ischemia, the femoral artery of each mouse was ligated and resected as previously described[32,33] (Figure 1A). Briefly,

mice were anesthetized with ketamine/xylazine and placed on a heating pad to maintain a proper body temperature. An incision was made on the underside of the mouse's left leg near the hip crease and adipose tissue and facia was separated to access to the femoral artery. The femoral artery was ligated immediately rostral to the internal iliac artery bifurcation and then a section of the femoral artery distal to this point was resected. Smaller bifurcations between the internal iliac bifurcation and the epigastric bifurcation were cauterized to prevent bleeding and the femoral artery was carefully separated from the femoral vein and the local skeletal muscle. The femoral artery was cauterized immediately caudal to the epigastric bifurcation to prevent bleeding and end the resection. The incision was closed using surgical staples. Mice were administered buprenorphine every twelve hours for the next 48 hours and water containing antibiotics and acetaminophen for the next 7 days to manage pain.

To quantify blood flow in each limb, mice were anesthetized with ketamine/xylazine or isofluorane and placed under a PeriScan PIM-II blood perfusion monitor (laser Doppler scanner) (Perimed, Inc. North Royalton, OH). Images were taken in triplicate. Regions of interest (ROIs) were traced around the ischemic and non-ischemic foot of each mouse to quantify perfusion intensity. Perfusion of the ischemic foot was normalized to the non-ischemic foot for each mouse. Perfusion was quantified at multiple time points including 1, 3, 7, 14, 21, and 28 days post-femoral artery ligation and resection.

Tissue processing

In general, mice were euthanized by CO_2 overdose. Blood was harvested via cardiac puncture and stored with 10 μL of 0.5 M EDTA to prevent coagulation. Mice were perfused through the left ventricle (after cutting the right atrium) with 10 mL PBS supplemented with heparin. All tissues harvested for RNA extraction were flash frozen in liquid nitrogen and stored at −80°C. In general, tissue harvest and processing procedures are based on previously-published methods[33,34].

Blood—For flow cytometry analysis of cell populations, 100 μL of blood was treated with AKC lysis buffer (Table S1) for 5 minutes, rotating. Lysis was quenched with FACS buffer and cells were spun down. Pellets were resuspended in FACS buffer to be stained for flow cytometry. To isolate plasma, blood samples were spun down at 5,000 g for 5 minutes at room temperature. Plasma was then transferred into a fresh tube and stored at −20°C.

Skeletal muscle—For flow cytometry analysis of cell populations, gastrocnemius muscles were placed in digestion buffer (Table S1), minced, and incubated at 37°C, shaking, for ~45 minutes. Digested tissue was then pipetted up and down to create a single-cell suspension, passed through a 70 μm filter, washed with FACS buffer, and pelleted. Cells were treated with AKC lysis buffer to lyse remaining red blood cells as needed. Cells were then stained for flow cytometry. For whole tissue analysis, gastrocnemius muscles were fixed in 4% PFA at 4°C, rotating, for 24–48 hours.

Flow cytometry and live cell sorting

All cells were stained with fluorophore-conjugated antibodies against cell surface proteins (Table S2) in FACS buffer or Brilliant Violet Stain Buffer (BD, if more than one Brilliant Violet fluorophore was used at one time) for 25 minutes at 4°C then washed with FACS buffer. For cell population analysis, cells were then stained with Live/Dead (Fisher) in PBS for 30 minutes at 4°C then washed with FACS buffer. Cells were then fixed with 2% PFA for 7–10 minutes at room temperature and washed with FACS buffer. Finally, cells were resuspended in FACS buffer and stored at 4°C until analyzed. Cells were run on the Attune Nxt (Thermofisher Scientific) and compensated and analyzed in FCS Express. For live cell sorting, cells were stained with 7AAD or DAPI prior to sorting on the FACSAria Fusion or Influx (BD Biosciences). Cells were sorted into RPMI media enriched with 20% FBS.

Histology

Preparing sections—Fixed skeletal muscles were incubated in 30% sucrose overnight at 4°C, rotating, until the tissues were saturated and sank to the bottom of the tube. Then, tissues were embedded in OCT and 10 μm sections were cut using a Cryostat (Leica Biosystems).

Immunofluorescence—Tissue sections were fixed once more in acetone for 10 minutes. Sections were then subjected to antigen retrieval and allowed to cool. They were then permeabilized with 0.25% Triton-100 in PBS, and then washed in PBS. Sections were blocked with 0.6% fish skin gelatin with 10% serum in PBS, then incubated with primary antibodies (Table S3) in 0.6% fish skin gelatin with 10% serum in PBS overnight at 4°C. Sections were washed as before and then incubated with secondary antibody for 1–2 hours at room temperature. Following one final wash, slides were counterstained with DAPI (1 μg/mL) and coverslipped using ProLong Gold (Life Technologies). Images were obtained using Zeiss LSM700 confocal microscope, 20X objective. Figures shown are maximal intensity projection images.

ELISA

Total IgM in mouse plasma and muscle lysates were measured using colorimetric ELISA (Tables S4, S5). EIA/RIA high-binding microplates were coated with IgM-specific antibody (SouthernBiotech, 1020–01). Mouse IgM standards (Southern Biotech, 0101–01) or plasma samples were detected with alkaline phosphatase-conjugated goat anti-mouse IgM secondary antibody (SouthernBiotech, 1020–04) and pNPP substrate (SouthernBiotech 0201–01). Absorbance measurements were analyzed with a SpectraMAX 190 microplate reader (Molecular Devices) at 405 nm. The standard curve was determined using a 4-parameter function and concentration measurements were extrapolated using Softmax Pro 3.1.2 software. Only samples with CV<15% and within the standard curve were included in analysis.

Gene expression

RNA extraction and cDNA synthesis—RNA was extracted from tissues and cells using TRIzol™ extraction (ThermoFisher Scientific, 15596026). 0.5 to 1 μg of RNA was

then treated with DNase (Invitrogen) and used to reverse transcribe cDNA using an iScript cDNA synthesis kit (BioRad, 1708891).

qRT-PCR—To quantify gene expression, cDNA was diluted in water as needed and combined with 0.5 mM forward and reverse primers (Table S6) and SYBR Green (SensiFast, BioLine). Semi-quantitative real-time PCR was performed on a CFX96 Real-Time System (BioRad) with an annealing temperature of 60°C for all reactions. Data were calculated by the ΔΔCt method and expressed in arbitrary units that were normalized to 18s levels.

Cell culture

B cell culture and conditioned media preparation—B-1a, B-1b, and B-2 cells were sorted from peritoneal lavage samples (Figure S1) on the FACSAria Fusion or Influx cell sorters (BD). They were then resuspended in TLR9 agonist treatment media at 500,000 cells per 250 μL for 7 days or in EC starvation media at the same cell:media ratio for 6 hours. Cultures were then spun down and conditioned media supernatants transferred to fresh tubes and stored at −20°C. Cell pellets were resuspended in TRIzol™ for RNA extraction.

Cell lines—Human umbilical vein endothelial cells were ordered from Lonza (C2519A) and cultured in EC growth media. Murine primary skeletal muscle endothelial cells were purchased from Cell Biologics (C57–6220) and cultured in complete mouse endothelial cell medium (Cell Biologics, M1168). Cells were passaged using TrypLE Express (Gibco, 12605–010). Experiments were conducted with cells passaged 2 to 5 times.

Proliferation and cell death assays—10,000 HUVECs were plated per well of a 96-well plate in 100 μL of EC starvation media for MTS assays and 60,000 murine ECs were plated per well of a 24-well plate in 400 μL of EC growth media for flow cytometric assessment of cell death and proliferation. Additional conditioned media treatments were added (specified in figure legends) and cells were then cultured in a hypoxia chamber (2% O_2, C-Chamber and ProOx C21, BioSpherix) within a cell culture incubator at 37°C for 24 hours.

For MTS assays only: At 23 hours, 20 μL of MTS reagent (Promega) was added to each well and the plate placed back in the hypoxia chamber for one additional hour. Absorbance from each well was then read with a SpectraMAX 190 microplate reader (Molecular Devices) at 490 nm and 665 nm. 665 nm values were subtracted from 490 nm to account for background. Blank control values were then subtracted from the absorbance values of each “non-blank” well and these values were normalized to the vehicle control.

For flow cytometry assays: Cells were trypsinized and spun down to wash away all treatments. Cells were then stained with Live/Dead Aqua (L34966A, Invitrogen) for 15 minutes on ice, followed by staining with an antibody specific to Ki67 (Table S2). The FoxP3 staining buffer kit (Invitrogen, 00-5523-00) was used to stain for Ki67 per manufacturer’s instructions. Cells were run on the Attune Nxt (ThermoFisher Scientific) following the first experiment and the Aurora Borealis (CyTEK) following the second experiment. Data was analyzed using FlowJo v10 (BD).

Statistics

All statistical analysis was performed using Prism 7 or 8 or 9 (GraphPad Software, Inc.). Because sample n < 15 for all murine experiments, normal distribution could not be determined. Mann-Whitney tests were used to compare two experimental groups and two-way ANOVAs were used to compare three or more experimental groups with two independent variables (such as both time and genotype, for example). Where experiments were conducted using male and female mice, statistical analyses were conducted separately by sex. Following two-way ANOVA, post-hoc Sidak's multiple comparisons test (with single pooled variance) was run to compare experimental groups. Normality and equal variance were not assessed as a pre-condition for this analysis. Data are generally expressed as mean ± standard deviation (SD). *P* values and the specific statistical analyses used are specified in figures and figure legends.

Results

Id3 regulated perfusion recovery in response to HLI in a B cell-specific manner

To investigate whether Id3 regulates blood flow in response to ischemia, HLI was surgically induced in Id3 knockout and wild type (WT) littermates (Figure 1A). At day 3 of HLI in wild type mice, *Id3* mRNA levels were significantly increased in ischemic (I) gastrocnemius muscles compared to non-ischemic (NI) muscles (Figure 1B). Using laser Doppler perfusion imaging (LDPI), we found that Id3 global knockout ($Id3^{GKO}$) mice had significantly reduced blood flow at days 14 and 21 after HLI compared to Id3 wild-type ($Id3^{GWT}$) littermates (Figure 1C). Histological staining verified that the injury response was isolated to the ischemic limb in these mice (Figure S2). Cell-specific Id3 knockout mice were employed to identify the cell type responsible for the attenuated perfusion recovery in $Id3^{GKO}$ mice. All lines were validated for effective and cell-specific knockout of Id3[8,23] (Figure S3). Interestingly, our hypothesis that loss of Id3 in ECs and macrophages would attenuate perfusion recovery proved null: male and female $Id3^{ECKO}$ (Figure S4A) and $Id3^{MKO}$ mice (Figure S4B) demonstrated no differences in perfusion recovery compared to WT littermate controls. However, B cell-specific Id3 KO mice ($Id3^{BKO}$) mice had significantly reduced blood flow recovery relative to $Id3^{BWT}$ controls at days 14 and 21 of HLI in males (Figure 1D) trending to be lower also in females at 14 and 21 days but only reaching statistical significance at day 28 of HLI in females (Figure S4C). The reason for these temporal differences are unclear, but it is of note that perfusion recovery in the male mice was higher than in the female and this has also been shown previously in the literature[35].

B-1b cell numbers were significantly increased in ischemic muscles of $Id3^{BKO}$ mice compared to $Id3^{BWT}$ mice

To identify the immune cell populations in I and NI skeletal muscles 7 days after HLI and test the impact of B cell-specific loss of Id3, flow cytometry of gastrocnemius muscles was performed (Figures 2A, S5, and S6C). We observed a significant increase in total $CD45^+$ immune cells (Figure 2B and S7A) as well as $CD19^+$ B cells (Figure 2C and S7B) in I muscle compared to NI muscle. The overall increase in immune cells was in part due to increases in B cell numbers, however, there were also significant increases in $CD11b^+F4/80^+$ macrophages (Figure S6E), $CD3^+$ T cells (Figure S6F), and other $CD11b^+$ immune cells

(Figure S6K) in Id3^{BWT} mice. However, while the numbers of total B cells in ischemic muscle were significantly higher in Id3^{BKO} mice compared to Id3^{BWT} mice (Figures 2C and S7B), as expected, total T cell, macrophage, neutrophil, monocyte, and other immune cell numbers were not significantly changed in Id3^{BKO} mice in I or NI muscles (Figures S6E–K and S7G–H).

The differences in B cell numbers were due to increases in CD19^{+}B220^{low} B-1 cells (Figures 3D and S7C), but not B220^{high} B-2 cells (Figures 2E and S7D). More specifically, CD5^{+} B-1a B cells (Figures 2F and S7E) were not affected by the loss of Id3 in B cells, but Id3^{BKO} mice had significantly more CD5^{-} B-1b cells (Figures 2G and S7F) in I muscle. B-1b cell numbers were also increased in spleen, bone marrow, and peritoneal cavity of Id3^{BKO} mice at day 7 of HLI (Figure S8). Our previous work demonstrated a similar B-1b-specific increase in these tissues at baseline in Apoe$^{-/-}$ mice fed a normal laboratory diet[23] suggesting that Id3-dependent increases in B-1b cell numbers in these compartments are not ischemia-dependent. Notably, however, there were no differences in total B cells or any of the B cell subtypes, including B-1b, in the skeletal muscle in the NI limb, providing evidence that Id3-dependent differences in B-1b cell number in skeletal muscle of the ischemic limb is not simply because the animal has more B-1b cells.

To explain why Id3^{BKO} mice have increased numbers of B-1b cells in ischemic muscle, we hypothesized that there were differences in cell recruitment to muscle. We observed a significant increase in *Cxcl12* transcripts from I gastrocnemius muscles on day 3 of HLI compared to NI controls (Figure 2H). We then investigated expression of CXCR4, the receptor for CXCL12, on B cell subsets in the peritoneal cavity. The peritoneal cavity is one of the niches in which B-1 cells reside. There, we observed that a higher proportion of B-1a, B-1b, and B-2 cell subsets from Id3^{BKO} mice were CXCR4^{+} at day 7 of HLI compared to WT littermate controls (Figure 2I). More importantly, when normalized to the number of WT B cell subsets that were CXCR4^{+}, Id3^{BKO} B-1b cells demonstrated the largest increase in the number of CXCR4^{+} cells compared to WT cells (Figure 2J). A similar pattern was observed for CXCR5^{+} B cells. The ligand for CXCR5 is CXCL13, which has been shown to be increased in the setting of ischemia[36]. The proportion of CXCR5^{+} B cell subsets was increased in Id3^{BKO} compared to WT littermate control mice at day 7 of HLI (Figure S9A), and that increase was most substantial in the B-1b cell compartment (Figure S9B). This provides an explanation for the finding that specifically B-1b cells increase in ischemic muscle of Id3^{BKO} mice.

Id3^{BKO} mice had higher levels of IgM in ischemic skeletal muscle and plasma during HLI compared to Id3^{BWT} mice.

B-1 cells are a major source of IgM *in vivo*[37] and prior studies suggest that expansion of the B-1b cell population *in vivo* will result in increased IgM levels[20,23]. We found that Id3^{BKO} mice had significantly higher levels of total IgM in circulation with a particularly significant spike in IgM levels at day 7 of HLI (Figure 3A). IgM levels were also increased locally in skeletal muscle after 7 days of HLI and this appeared to persist until day 28 of HLI (Figure 3B). IgM can be identified in ischemic skeletal muscle by immunofluorescence as

well (Figure 3C). Additionally, circulating levels of total IgG, IgG1, IgG2a, IgG2b, IgG2c, and IgG3 were not different between genotypes after 7 days of HLI (Figure S10).

Prior work in the setting of atherosclerosis demonstrates that B-1 cells secrete natural IgMs that are specific to various danger-associated molecular patterns (DAMPs) upregulated in the setting of hyperlipidemia, including oxidized lipids[23,38–41]. DAMPs such as High mobility group box-1 (HMGB1) and oxidized phospholipid 1-palmitoyl-2-arachidonoyl-sn-glycero-3-phosphocholine (oxPAPC) have been shown to have pro-angiogenic effects in ECs and affect blood flow recovery during HLI[42–50]. To investigate whether HMGB1- and oxPAPC-specific IgM (Figure S11A) were present in the setting of ischemia and upregulated in $Id3^{BKO}$ mice, IgM levels were measured by ELISA. IgM specific to HMGB1 (Figure S11B) and oxPAPC (Figure S11C) were significantly higher in the plasma of $Id3^{BKO}$ mice at day 7 of HLI.

Conditioned media from B-1b cells with IgM secreting capabilities inhibited EC proliferation and survival in response to hypoxia

To begin investigating whether B-1-produced IgM affects vascular function in the setting of hypoxia, we asked whether B cell-produced IgM had paracrine effects on ECs in the setting of hypoxia. Secreted IgM (sIgM)-deficient mice have altered B cell populations *in vivo* introducing important caveats restricting our use of the HLI model in this mouse[51–53]. Thus, we selected an *in vitro* model that would eliminate these additional variables. We verified that our cultured ECs expressed EC marker CD31 (Figure S12A) as well as IgM receptors FcμR and pIgR, but not Fcα/μR, in the settings of hypoxia and normoxia (Figure S12B). ECs were cultured with conditioned media (CM) from $sIgM^{+/+}$ or $sIgM^{-/-}$ B-1b or B-1a cells. B-1a and B-1b CM treatments both contained 5 μg/mL of IgM and equal volumes were used for $sIgM^{-/-}$ B-1a and B-1b CM treatments to ensure that cells were exposed to equal amounts of other media components. EC numbers were quantified using an MTS assay (Figure 4A). While ECs cultured with CM from $sIgM^{+/+}$ and $sIgM^{-/-}$ B-1a cells did not affect cell numbers compared to media-only controls, we observed that CM from WT B-1b cells, but not $sIgM^{-/-}$ B-1b cells attenuated EC numbers (Figure 4B). ECs were then cultured with WT B-1b media to quantify proliferation and cell death in the setting of hypoxia. IgM-containing B-1b CM reduced the percentage of $Ki67^{+}$ ECs in culture as well as the Ki67 mean fluorescence intensity over control CM (Figure 4C). Additionally, the proportion of dead ECs was increased in B-1b CM-treated cultures (Figure 4D). Altogether, these data indicate a role for B-1b cell-secreted IgM in regulating EC proliferation and survival in the setting of hypoxia *in vitro*.

$Id3^{BKO}$ mice demonstrated reduced vascular density in the tibialis anterior muscle during HLI

To determine if our *in vitro* findings translated to changes in the vasculature *in vivo*, vascular density was quantified in the tibialis anterior (TA) muscle at Day 28 of HLI in $Id3^{BWT}$ and $Id3^{BKO}$ mice. Vascular density was quantified by counting the number of total $CD31^{+}$ vessels, $\alpha SMA^{-}CD31^{+}$ capillaries (Figure 5A, arrowheads) and $\alpha SMA^{+}CD31^{+}$ arteries and arterioles (Figure 5A, arrows) per image. Five images were captured per muscle section, and three sections 300 μm apart in each muscle were imaged per mouse. The number of

CD31$^+$ structures, or vessels, per muscle section were quantified and averaged amongst all muscles in the same experimental group and also plotted per section to better describe density across each muscle (Figure S13A). The average density of total CD31$^+$ vessels was significantly lower in the I TA muscles of Id3^{BKO} mice than Id3^{BWT} controls (Figure 5C) mirroring the reductions in cultured EC numbers when treated with sIgM$^{+/+}$ B-1b CM (Figure 4B–D). When plotted across the length of the muscle (Figure S13B), total CD31$^+$ density was also significantly reduced in Id3^{BKO} I TA muscles (Figure S13C). Interestingly, we observed differences when CD31$^+$ vessels were divided between those with and without investment of αSMA$^+$ cells (pericytes and vascular smooth muscle cells (VSMCs)). The average αSMA$^-$CD31$^+$ capillary density per muscle was not different between genotypes in (Figures 5C), nor was the area under the curve when capillary densities were plotted across sections per TA (Figure S13D–E). However, TA-specific reductions in the density of αSMA$^+$CD31$^+$ vessels were observed in I Id3^{BKO} muscles compared to I Id3^{BWT} muscles (Figures 5D, S13F–G).

Additionally, increased vascular permeability suggests decreased vascular stability and thus potentially lower perfusion. Early signs of edema and vascular permeability were assessed by quantifying the wet and dry weights of TA muscles after 7 days of HLI. While edema clearly increased with ischemia, there was no difference between genotypes (Figure S14).

Discussion

PAD patients with insufficient neovascularization capacity do not have access to many effective therapeutic options due to a lack of understanding about the mechanisms driving these adaptations. Using a murine model of ischemia, we identified Id3, IgM, and B cells, respectively, as novel molecular and cellular regulators of ischemic neovascularization. More specifically, mice lacking Id3 expression in B cells, but not ECs or macrophages, demonstrated attenuated blood flow recovery in the setting of HLI.

Our study provides the first evidence that B cells play a role in mediating ischemic neovascularization. Klotzsche-von Ameln *et al.* demonstrated that Del-1$^{-/-}$ mice have increased B and T cell recruitment to skeletal muscle and reduced blood flow recovery after HLI; however, the study did not demonstrate specifically that B cells were mediating blood flow changes or neovascularization[54]. Two additional studies demonstrated that exogenous delivery of an anti-VEGFA IgG antibody can inhibit capillary density and blood flow recovery during HLI via interactions with FcɣR on myeloid cells[55,56]. It remains unclear, however, how much this FcɣR signaling axis affects neovascularization at homeostatic levels. B cells and IgM have also been implicated in promoting tissue injury during ischemia/reperfusion via complement deposition[57–64]. This injury model, however, lacks a chronic time point in which to observe and quantify a neovascular component. Results from studies demonstrating a role for FcɣR in neovascularization and our findings that cultured ECs express IgM receptors FcμR and pIgR prompt further questions regarding the role that IgM receptors on endothelium might play in the growth of new blood vessels. It is unknown if these receptors are expressed on endothelium or other vascular cells of human skeletal muscle. Studies specifically investigating the expression of IgM and IgM receptors in human

skeletal muscle of PAD patients, however, will be necessary for full translation of this study into human PAD.

Loss of Id3 in B cells attenuated blood flow at later time points during HLI and this correlated with early increases in B-1b cell numbers in ischemic muscle, but not non-ischemic muscle, and increased IgM levels in circulation and ischemic muscle. Previous literature demonstrated that IgM deposition activated complement and myocyte damage in ischemic skeletal muscle[58,59,63]. A recent study demonstrated that myocyte signaling can influence vascular responses in the skeletal muscle[65]; but, interestingly, our studies provide evidence that IgM can also directly influence the endothelium in the absence of myocytes. *In vitro* studies revealed that conditioned media from B-1b cells that secrete IgM inhibited EC proliferation and survival, while conditioned media from secreted IgM-deficient B-1b cells did not. EC survival and proliferation are necessary for in both arteriogenesis and angiogenesis[66–69] as well as to prevent vascular dropout in hypoxic tissue. Furthermore, this effect was specific to IgM-secreting B-1b cells as $sIgM^{+/+}$ and $sIgM^{-/-}$ B-1a CM did not have differential effects on EC numbers *in vitro*. This raises an interesting question regarding the distinctions between these two B cell subsets and the IgM repertoire secreted by each. Previous studies demonstrated distinctions in IgH rearrangement, heavy chain variable domain family usage, and frequency of N-sequence additions during rearrangements between B-1a and B-1b cells[70–72]. While additional studies are needed to understand the implications of these published findings for the current study, results support a functional distinction between B-1a and B-1b cells and rationalizes pursuit of a deeper understanding for B-1 cell subsets in ischemia and neovascularization.

The total number of $CD31^+$ blood vessels and those specifically with αSMA^+ cell investment were also decreased in ischemic TA muscles of $Id3^{BKO}$ mice, demonstrating loss of Id3 in B cells affects the number of stabilized blood vessels in ischemic muscle. We suggest that inhibition of EC population size and frequency of stabilized blood vessels by increased levels of IgM in $Id3^{BKO}$ mice is at least in part a cause of attenuated blood flow recovery in our model.

In addition to total IgM, DAMP-specific IgM levels were also increased. These DAMPs, HMGB1 and oxPAPC, promote neovascularization and are upregulated in the setting of ischemia[42–50]. More specifically, HMGB1 exogenously delivered during HLI was shown to promote blood flow recovery[73]. A study was recently published demonstrating that peritoneal B-1 cells are the main source of HMGB1-specific IgM, which neutralizes HMGB1 function *in vivo*[74]. Thus, it is possible that beyond inhibiting EC number directly, increased levels of IgM specific to these molecules may result in increased IgM-DAMP binding, which in turn inhibits DAMP-induced mechanisms that normally promote blood flow recovery. Overall, these hypotheses and our *in vitro* results introduce a potential novel role for IgM in regulating endothelial cell responses during ischemic neovascularization.

Approaches to specifically deplete B-1b cells or IgM in wild type mice are not yet developed. A B-1b cell-specific marker has not been identified: the markers typically used to identify this subset (CD5, B220, CD19, CD11b, CD23) are also expressed on other cell types making depletion methods currently unfeasible. And while studies have

successfully reduced IgG or IgM *in vivo* by passing blood through a column to deplete the antibodies[75–78], these methods do not permit facile depletion over time. Furthermore, while anti-CD20 antibodies have been used to deplete B cells *in vivo*, these methods are not completely effective: B-1 B cells persist at low levels in the peritoneal cavity following antibody administration[79]. Adoptive transfer studies are a feasible alternative; however, prior studies demonstrate that transfer of B cells into B cell-deficient mice has low transfer efficiency[80]. While transfers into $Rag1^{-/-}$ mice are more effective, T cell populations are then absent in the model and these cells have been shown to also play an important role in ischemic neovascularization[28,81,82]. Further development of these methods will be of great importance for advancing our understanding of the roles B-1 cells, and specifically B-1b cells, play during ischemia and other disease and injury settings.

When considering how to translate these mechanisms to human disease, it is important to identify distinctions between our model of HLI and human disease. First, the HLI model employed in this study is an acute model relative to the long-term, chronic timeline characteristic of PAD in humans. Following surgery, mice lose approximately 70% of the blood flow in the foot of the affected leg. However, PAD is often caused by atherosclerosis, which develops on the order of years, in a major artery feeding the lower limb[2,83]. Second, the immune systems of mice and humans are not the same. To date, a putative B-1 cell population has been identified in humans[84], however, further investigation is required to fully understand the identity and function of B-1 cells and how they regulate ischemic neovascularization in humans.

In summary, these studies are the first to demonstrate that loss of Id3 leads to impaired perfusion recovery after HLI and determine that this is a B cell-intrinsic effect. The findings that $Id3^{BKO}$ mice with reduced blood flow recovery during HLI had increased B-1b cell numbers and IgM levels in the skeletal muscle, coupled with *in vitro* data demonstrating that B-1b-derived IgM inhibited EC proliferation and survival in the setting of hypoxia provides a novel mechanistic link between Id3, B cells, and HLI. Further studies to determine the impact of loss of B-1b cells and their IgM products on angiogenesis and recovery of perfusion after HLI could lead to novel targeted immune approaches to improve symptoms and outcomes in PAD patients.

Supplementary Material

Refer to Web version on PubMed Central for supplementary material.

Acknowledgments

The authors would like to acknowledge the University of Virginia Flow Cytometry Core for providing training, equipment, and technical support in the conductance of live sorting and acquisition of flow cytometry data as well as the University of Virginia Advanced Microscopy Facility for training, equipment, and technical support. The authors would also like to thank R. John Lye and Daniel Hess for assistance with and advice on the HLI procedure and immunofluorescence assays. Thanks also goes to Hema Kothari who provided valuable insights and resources for *in vitro* culture work presented in this study. Finally, the authors thank the laboratory of Richard Price for providing equipment and training for conducting laser Doppler perfusion imaging assays. Servier Medical Art was used in the creation of some figures (smart.servier.com).

Sources of Funding

These studies were supported by R01HL136098, R01HL141123 and R01HL48109 (CAM); 1R01HL141325-01, 1R01HL148590-01, 1R01HL150003-01, 3R01HL101200-11, 1R01GM129074-01 (BHA); 5R01HL146673-03 (VCG); AHA 18CDA34110392 (PS); AHA 16PRE30770007, and T32 HL007284 grants (VO).

Abbreviations:

αSMA	alpha-smooth muscle actin
BKO	B cell-specific knockout genotype
BWT	B cell-specific wild-type genotype
CM	conditioned media
EC	endothelial cell
ECKO	endothelial cell-specific knockout genotype
ECWT	endothelial cell-specific wild-type genotype
GKO	global knockout genotype
GWT	global wild-type genotype
HLI	hind limb ischemia
I	ischemic
Id3	Inhibitor of differentiation 3
IgM	Immunoglobulin M
MKO	macrophage-specific knockout genotype
MWT	macrophage-specific wild-type genotype
NI	non-ischemic
sIgM	secreted IgM
VSMC	vascular smooth muscle cell
TA	Tibialis anterior

References

1. Fowkes FG, Aboyans V, Fowkes FJ, McDermott MM, Sampson UK, Criqui MH. Peripheral artery disease: epidemiology and global perspectives. Nat Rev Cardiol. 2017;14:156–170. [PubMed: 27853158]
2. Annex BH, Beller GA. Towards the Development of Novel Therapeutics for Peripheral Artery Disease. Trans Am Clin Clim. Assoc 2016;127:224–234.
3. Benjamin EJ, Muntner P, Alonso A, et al. Heart Disease and Stroke Statistics-2019 Update: A Report From the American Heart Association. Circulation. 2019;139:e56–e528. [PubMed: 30700139]

4. Castro PR, Barbosa AS, Pereira JM, Ranfley H, Felipetto M, Gonçalves CAX, Paiva IR, Berg BB, Barcelos LS. Cellular and Molecular Heterogeneity Associated with Vessel Formation Processes. Biomed Res. Int. 2018;2018:1–32.
5. Brevetti G, Giugliano G, Brevetti L, Hiatt WR. Inflammation in peripheral artery disease. Circulation. 2010;122:1862–1875. [PubMed: 21041698]
6. Carmelli D, Fabsitz RR, Swan GE, Reed T, Miller B, Wolf PA. Contribution of genetic and environmental influences to ankle-brachial blood pressure index in the NHLBI Twin Study. National Heart, Lung, and Blood Institute. Am J Epidemiol. 2000;151:452–458. [PubMed: 10707913]
7. Forrest ST, Taylor AM, Sarembock IJ, Perlegas D, McNamara CA. Phosphorylation regulates Id3 function in vascular smooth muscle cells. Circ Res. 2004;95:557–559. [PubMed: 15321928]
8. Kaplan JL, Marshall MA, C CM, Harmon DB, Garmey JC, Oldham SN, Hallowell P, McNamara CA. Adipocyte progenitor cells initiate monocyte chemoattractant protein-1-mediated macrophage accumulation in visceral adipose tissue. Mol Metab. 2015;4:779–794. [PubMed: 26629403]
9. Ling F, Kang B, Sun XH. Id proteins: small molecules, mighty regulators. Curr Top Dev Biol. 2014;110:189–216. [PubMed: 25248477]
10. Nickenig G, Baudler S, Muller C, Werner C, Werner N, Welzel H, Strehlow K, Bohm M. Redox-sensitive vascular smooth muscle cell proliferation is mediated by GKLF and Id3 in vitro and in vivo. FASEB J. 2002;16:1077–1086. [PubMed: 12087069]
11. Zhang X, Ai F, Li X, et al. Inflammation-induced S100A8 activates Id3 and promotes colorectal tumorigenesis. Int J Cancer. 2015;137:2803–2814. [PubMed: 26135667]
12. Taylor AM, Li F, Thimmalapura P, Gerrity RG, Sarembock IJ, Forrest S, Rutherford S, McNamara CA. Hyperlipemia and oxidation of LDL induce vascular smooth muscle cell growth: an effect mediated by the HLH factor Id3. J Vasc Res. 2006;43:123–130. [PubMed: 16340216]
13. Manichaikul A, Rich SS, Perry H, et al. A functionally significant polymorphism in ID3 is associated with human coronary pathology. PLoS One. 2014;9:e90222. [PubMed: 24603695]
14. Doran AC, Lehtinen AB, Meller N, et al. Id3 is a novel atheroprotective factor containing a functionally significant single-nucleotide polymorphism associated with intima-media thickness in humans. Circ Res. 2010;106:1303–1311. [PubMed: 20185798]
15. Cutchins A, Harmon DB, Kirby JL, et al. Inhibitor of differentiation-3 mediates high fat diet-induced visceral fat expansion. Arter. Thromb Vasc Biol 2012;32:317–324.
16. Lyden D, Young AZ, Zagzag D, et al. Id1 and Id3 are required for neurogenesis, angiogenesis and vascularization of tumour xenografts. Nature. 1999;401:670–677. [PubMed: 10537105]
17. Clever JL, Sakai Y, Wang RA, Schneider DB. Inefficient skeletal muscle repair in inhibitor of differentiation knockout mice suggests a crucial role for BMP signaling during adult muscle regeneration. Am. J. Physiol. Physiol. 2010;298:C1087–C1099.
18. Lee D, Shenoy S, Nigatu Y, Plotkin M. Id Proteins Regulate Capillary Repair and Perivascular Cell Proliferation following Ischemia-Reperfusion Injury. PLoS One. 2014;9:e88417. [PubMed: 24516656]
19. Murre C Helix–loop–helix proteins and the advent of cellular diversity: 30 years of discovery. Genes Dev. 2019;33:6–25. [PubMed: 30602438]
20. Doran AC, Lipinski MJ, Oldham SN, et al. B-cell aortic homing and atheroprotection depend on Id3. Circ Res. 2012;110:e1–12. [PubMed: 22034493]
21. Srikakulapu P, Upadhye A, Rosenfeld SM, et al. Perivascular Adipose Tissue Harbors Atheroprotective IgM-Producing B Cells. Front Physiol. 2017;8:719. [PubMed: 28970806]
22. Perry H B cell subsets in atherosclerosis. Front. Immunol. 2012;3.
23. Rosenfeld SM, Perry HM, Gonen A, et al. B-1b Cells Secrete Atheroprotective IgM and Attenuate Atherosclerosis. Circ Res. 2015;117:e28–39. [PubMed: 26082558]
24. Lopez-Pastrana J, Ferrer LM, Li YF, et al. Inhibition of Caspase-1 Activation in Endothelial Cells Improves Angiogenesis: A NOVEL THERAPEUTIC POTENTIAL FOR ISCHEMIA. J Biol Chem. 2015;290:17485–17494. [PubMed: 26037927]
25. Cohen RA, Murdoch CE, Watanabe Y, et al. Endothelial Cell Redox Regulation of Ischemic Angiogenesis. J Cardiovasc Pharmacol. 2016;67:458–464. [PubMed: 26927696]

26. Capoccia BJ, Gregory AD, Link DC. Recruitment of the inflammatory subset of monocytes to sites of ischemia induces angiogenesis in a monocyte chemoattractant protein-1-dependent fashion. J Leukoc Biol. 2008;84:760–768. [PubMed: 18550788]
27. Krishnasamy K, Limbourg A, Kapanadze T, et al. Blood vessel control of macrophage maturation promotes arteriogenesis in ischemia. Nat Commun. 2017;8:952. [PubMed: 29038527]
28. Hellingman AA, Zwaginga JJ, van Beem RT, Te RMSMC, Hamming JF, Fibbe WE, Quax PH, Geutskens SB. T-cell-pre-stimulated monocytes promote neovascularisation in a murine hind limb ischaemia model. Eur J Vasc Endovasc Surg. 2011;41:418–428. [PubMed: 21193337]
29. Brechot N, Gomez E, Bignon M, et al. Modulation of macrophage activation state protects tissue from necrosis during critical limb ischemia in thrombospondin-1-deficient mice. PLoS One. 2008;3:e3950. [PubMed: 19079608]
30. Hsieh PL, Rybalko V, Baker AB, Suggs LJ, Farrar RP. Recruitment and therapeutic application of macrophages in skeletal muscles after hind limb ischemia. J Vasc Surg. 2018;67:1908–1920 e1. [PubMed: 29273298]
31. Gadomski S, Singh SK, Singh S, et al. Id1 and Id3 Maintain Steady-State Hematopoiesis by Promoting Sinusoidal Endothelial Cell Survival and Regeneration. Cell Rep.. 2020;31:107572. [PubMed: 32348770]
32. Ganta VC, Choi MH, Kutateladze A, Fox TE, Farber CR, Annex BH. A MicroRNA93–Interferon Regulatory Factor-9–Immunoresponsive Gene-1–Itaconic Acid Pathway Modulates M2-Like Macrophage Polarization to Revascularize Ischemic Muscle. Circulation. 2017;135:2403–2425. [PubMed: 28356443]
33. Ganta VC, Choi M, Farber CR, Annex BH. Antiangiogenic VEGF 165 b Regulates Macrophage Polarization via S100A8/S100A9 in Peripheral Artery Disease. Circulation. 2019;139:226–242. [PubMed: 30586702]
34. Osinski V, Bauknight DK, Dasa SSK, et al. In vivo liposomal delivery of PPARα/γ dual agonist tesaglitazar in a model of obesity enriches macrophage targeting and limits liver and kidney drug effects. Theranostics. 2020;10:585–601. [PubMed: 31903139]
35. Peng X, Wang J, Lassance-Soares RM, et al. Gender differences affect blood flow recovery in a mouse model of hindlimb ischemia. Am. J. Physiol. Circ. Physiol. 2011;300:H2027–H2034.
36. Chen J, Crispin JC, Tedder TF, Dalle Lucca J, Tsokos GC. B cells contribute to ischemia/reperfusion-mediated tissue injury. J Autoimmun. 2009;32:195–200. [PubMed: 19342197]
37. Baumgarth N, Herman OC, Jager GC, Brown L, Herzenberg LA, Herzenberg LA. Innate and acquired humoral immunities to influenza virus are mediated by distinct arms of the immune system. Proc Natl Acad Sci U S A. 1999;96:2250–2255. [PubMed: 10051627]
38. Zou J, Wang G, Li H, Yu X, Tang C. IgM natural antibody T15/E06 in atherosclerosis. Clin. Chim. Acta 2020;504:15–22. [PubMed: 31991130]
39. Hörkkö S, Bird DA, Miller E, et al. Monoclonal autoantibodies specific for oxidized phospholipids or oxidized phospholipid–protein adducts inhibit macrophage uptake of oxidized low-density lipoproteins. J. Clin. Invest. 1999;103:117–128. [PubMed: 9884341]
40. Tsimikas S, Miyanohara A, Hartvigsen K, et al. Human Oxidation-Specific Antibodies Reduce Foam Cell Formation and Atherosclerosis Progression. J. Am. Coll. Cardiol. 2011;58:1715–1727. [PubMed: 21982317]
41. Chang M-K, Binder CJ, Miller YI, Subbanagounder G, Silverman GJ, Berliner JA, Witztum JL. Apoptotic Cells with Oxidation-specific Epitopes Are Immunogenic and Proinflammatory. J. Exp. Med. 2004;200:1359–1370. [PubMed: 15583011]
42. Jeong J, Lee J, Lim J, Cho S, An S, Lee M, Yoon N, Seo M, Lim S, Park S. Soluble RAGE attenuates AngII-induced endothelial hyperpermeability by disrupting HMGB1-mediated crosstalk between AT1R and RAGE. Exp Mol Med. 2019;51:113.
43. De Mori R, Straino S, Di Carlo A, Mangoni A, Pompilio G, Palumbo R, Bianchi ME, Capogrossi MC, Germani A. Multiple effects of high mobility group box protein 1 in skeletal muscle regeneration. Arter. Thromb Vasc Biol 2007;27:2377–2383.
44. Fiuza C, Bustin M, Talwar S, Tropea M, Gerstenberger E, Shelhamer JH, Suffredini AF. Inflammation-promoting activity of HMGB1 on human microvascular endothelial cells. Blood. 2003;101:2652–2660. [PubMed: 12456506]

45. Jiang R, Cai J, Zhu Z, et al. Hypoxic trophoblast HMGB1 induces endothelial cell hyperpermeability via the TRL-4/caveolin-1 pathway. J Immunol. 2014;193:5000–5012. [PubMed: 25339669]
46. Luo Y, Li SJ, Yang J, Qiu YZ, Chen FP. HMGB1 induces an inflammatory response in endothelial cells via the RAGE-dependent endoplasmic reticulum stress pathway. Biochem Biophys Res Commun. 2013;438:732–738. [PubMed: 23911608]
47. Lv B, Wang H, Tang Y, Fan Z, Xiao X, Chen F. High-mobility group box 1 protein induces tissue factor expression in vascular endothelial cells via activation of NF-kappaB and Egr-1. Thromb Haemost. 2009;102:352–359. [PubMed: 19652887]
48. Singh B, Biswas I, Bhagat S, Surya Kumari S, Khan GA. HMGB1 facilitates hypoxia-induced vWF upregulation through TLR2-MYD88-SP1 pathway. Eur J Immunol. 2016;46:2388–2400. [PubMed: 27480067]
49. Yang S, Xu L, Yang T, Wang F. High-mobility group box-1 and its role in angiogenesis. J Leukoc Biol. 2014;95:563–574. [PubMed: 24453275]
50. Bochkov VN, Philippova M, Oskolkova O, et al. Oxidized phospholipids stimulate angiogenesis via autocrine mechanisms, implicating a novel role for lipid oxidation in the evolution of atherosclerotic lesions. Circ Res. 2006;99:900–908. [PubMed: 16973904]
51. Boes M, Esau C, Fischer MB, Schmidt T, Carroll M, Chen J. Enhanced B-1 cell development, but impaired IgG antibody responses in mice deficient in secreted IgM. J. Immunol. 1998;160:4776–87. [PubMed: 9590224]
52. Ehrenstein MR, O'Keefe TL, Davies SL, Neuberger MS. Targeted gene disruption reveals a role for natural secretory IgM in the maturation of the primary immune response. Proc. Natl. Acad. Sci. 1998;95:10089–10093. [PubMed: 9707605]
53. Lino AC, Mohr E, Demengeot J. Naturally secreted immunoglobulins limit B1 and MZ B-cell numbers through a microbiota-independent mechanism. Blood. 2013;122:209–218. [PubMed: 23723451]
54. Klotzsche-von Ameln A, Cremer S, Hoffmann J, et al. Endogenous developmental endothelial locus-1 limits ischaemia-related angiogenesis by blocking inflammation. Thromb Haemost. 2017;117:1150–1163. [PubMed: 28447099]
55. Yasuma R, Cicatiello V, Mizutani T, et al. Intravenous immune globulin suppresses angiogenesis in mice and humans. Signal Transduct Target Ther. 2016;1.
56. Bogdanovich S, Kim Y, Mizutani T, et al. Human IgG1 antibodies suppress angiogenesis in a target-independent manner. Signal Transduct Target Ther. 2016;1.
57. van der Pol P, Roos A, Berger SP, Daha MR, van Kooten C. Natural IgM antibodies are involved in the activation of complement by hypoxic human tubular cells. Am J Physiol Ren. Physiol 2011;300:F932–40.
58. Austen WG Jr., Zhang M, Chan R, Friend D, Hechtman HB, Carroll MC, Moore FD Jr.. Murine hindlimb reperfusion injury can be initiated by a self-reactive monoclonal IgM. Surgery. 2004;136:401–406. [PubMed: 15300207]
59. Chan RK, Ding G, Verna N, Ibrahim S, Oakes S, Austen WG Jr., Hechtman HB, Moore FD Jr.. IgM binding to injured tissue precedes complement activation during skeletal muscle ischemia-reperfusion. J Surg Res. 2004;122:29–35. [PubMed: 15522311]
60. Zhang M, Austen WG Jr., Chiu I, et al. Identification of a specific self-reactive IgM antibody that initiates intestinal ischemia/reperfusion injury. Proc Natl Acad Sci U S A. 2004;101:3886–3891. [PubMed: 14999103]
61. Weiser MR, Williams JP,Moore FD Jr., Kobzik L, Ma M, Hechtman HB, Carroll MC. Reperfusion injury of ischemic skeletal muscle is mediated by natural antibody and complement. J Exp Med. 1996;183:2343–2348. [PubMed: 8642343]
62. Williams JP, Pechet TT, Weiser MR, Reid R, Kobzik L, Moore FD Jr., Carroll MC, Hechtman HB. Intestinal reperfusion injury is mediated by IgM and complement. J Appl Physiol. 1999;86:938–942. [PubMed: 10066708]
63. Sheu EG, Oakes SM, Ahmadi-Yazdi C, Afnan J, Carroll MC, Moore FD Jr.. Restoration of skeletal muscle ischemia-reperfusion injury in humanized immunodeficient mice. Surgery. 2009;146:340–346. [PubMed: 19628094]

64. Zhang M, Michael LH, Grosjean SA, Kelly RA, Carroll MC, Entman ML. The role of natural IgM in myocardial ischemia-reperfusion injury. J Mol Cell Cardiol. 2006;41:62–67. [PubMed: 16781728]

65. Latroche C, Weiss-Gayet M, Muller L, et al. Coupling between Myogenesis and Angiogenesis during Skeletal Muscle Regeneration Is Stimulated by Restorative Macrophages. Stem Cell Reports. 2017;9:2018–2033. [PubMed: 29198825]

66. Weckbach L, Preissner K, Deindl E. The Role of Midkine in Arteriogenesis, Involving Mechanosensing, Endothelial Cell Proliferation, and Vasodilation. Int. J. Mol. Sci. 2018;19:2559.

67. Cai W, Schaper W. Mechanisms of arteriogenesis. Acta Biochim. Biophys. Sin. (Shanghai). 2008;40:681–692. [PubMed: 18685784]

68. Moraes F, Paye J, Mac Gabhann F, Zhuang ZW, Zhang J, Lanahan AA, Simons M. Endothelial Cell–Dependent Regulation of Arteriogenesis. Circ. Res. 2013;113:1076–1086. [PubMed: 23897694]

69. Adams RH, Alitalo K. Molecular regulation of angiogenesis and lymphangiogenesis. Nat Rev Mol Cell Biol. 2007;8:464–478. [PubMed: 17522591]

70. Kantor AB, Merrill CE, Herzenberg LA, Hillson JL. An unbiased analysis of V(H)-D-J(H) sequences from B-1a, B-1b, and conventional B cells. J. Immunol. 1997;158:1175–86. [PubMed: 9013957]

71. Tornberg UC, Holmberg D. B-1a, B-1b and B-2 B cells display unique VHDJH repertoires formed at different stages of ontogeny and under different selection pressures. EMBO J.. 1995;14:1680–1689. [PubMed: 7737121]

72. Prohaska TA, Que X, Diehl CJ, Hendrikx S, Chang MW, Jepsen K, Glass CK, Benner C, Witztum JL. Massively Parallel Sequencing of Peritoneal and Splenic B Cell Repertoires Highlights Unique Properties of B-1 Cell Antibodies. J. Immunol. 2018;200:1702–1717. [PubMed: 29378911]

73. Sachdev U, Cui X, Hong G, Namkoong S, Karlsson JM, Baty CJ, Tzeng E. High mobility group box 1 promotes endothelial cell angiogenic behavior in vitro and improves muscle perfusion in vivo in response to ischemic injury. J Vasc Surg. 2012;55:180–191. [PubMed: 21944908]

74. Geng Y, Munirathinam G, Palani S, Ross JE, Wang B, Chen A, Zheng G. HMGB1-Neutralizing IgM Antibody Is a Normal Component of Blood Plasma. J. Immunol. 2020;205:407–413. [PubMed: 32522835]

75. Soares Mp, Latinne D, Elsen M, Figueroa J, Bach Fh, Bazin H. In vivo depletion of xenoreactive natural antibodies with an anti-mu monoclonal antibody. Transplantation. 1993;56:1427–1432. [PubMed: 8279015]

76. Seijsing J, Yu S, Frejd FY, Höiden-Guthenberg I, Gräslund T. In vivo depletion of serum IgG by an affibody molecule binding the neonatal Fc receptor. Sci. Rep. 2018;8:5141. [PubMed: 29572538]

77. Lucchiari N, Azimzadeh A, Wolf P, Regnault V, Cinqualbre J. In Vivo and In Vitro Optimization of Depletion of IgM and IgG Xenoantibodies by Immunoadsorption Using Cell Membrane Proteins. Artif. Organs 2008;21:278–286.

78. Xu Y, Lorf T, Sablinski T, Gianello P, Bailin M, Monroy R, Kozlowski T, Awwad M, Cooper DKC, Sachs DH. Removal of anti-porcine natural antibodies from human and nonhuman primate plasma in vitro and in vivo by a gal-alpha1-3gal-beta1-4beta-Glc-x immunoaffinity column. Transplantation. 1998;172–179. [PubMed: 9458010]

79. Schaheen B, Downs EA, Serbulea V, et al. B-Cell Depletion Promotes Aortic Infiltration of Immunosuppressive Cells and Is Protective of Experimental Aortic Aneurysm. Arter. Thromb Vasc Biol. 2016;36:2191–2202.

80. Baumgarth N, Jager GC, Herman OC, Herzenberg LA, Herzenberg LA. CD4+ T cells derived from B cell-deficient mice inhibit the establishment of peripheral B cell pools. Proc. Natl. Acad. Sci. 2000;97:4766–4771. [PubMed: 10781082]

81. Stabile E, Kinnaird T, la Sala A, et al. CD8+ T lymphocytes regulate the arteriogenic response to ischemia by infiltrating the site of collateral vessel development and recruiting CD4+ mononuclear cells through the expression of interleukin-16. Circulation. 2006;113:118–124. [PubMed: 16380545]

82. Kwee BJ, Budina E, Najibi AJ, Mooney DJ. CD4 T-cells regulate angiogenesis and myogenesis. Biomaterials. 2018;178:109–121. [PubMed: 29920403]

83. Annex BH. Therapeutic angiogenesis for critical limb ischaemia. Nat Rev Cardiol. 2013;10:387–396. [PubMed: 23670612]

84. Rothstein TL, Quach TD. The human counterpart of mouse B-1 cells. Ann N Y Acad Sci. 2015;1362:143–152. [PubMed: 25988790]

Highlights

- Global- and B cell-specific, but not EC- or macrophage-, specific loss of Id3 attenuates blood flow recovery in the setting of hind limb ischemia.
- B cell-specific Id3 KO mice have increased B-1b cell numbers and IgM levels and attenuated vascular density in ischemic muscle.
- Conditioned media from B-1b cells that secrete IgM inhibits EC proliferation and survival *in vitro*.

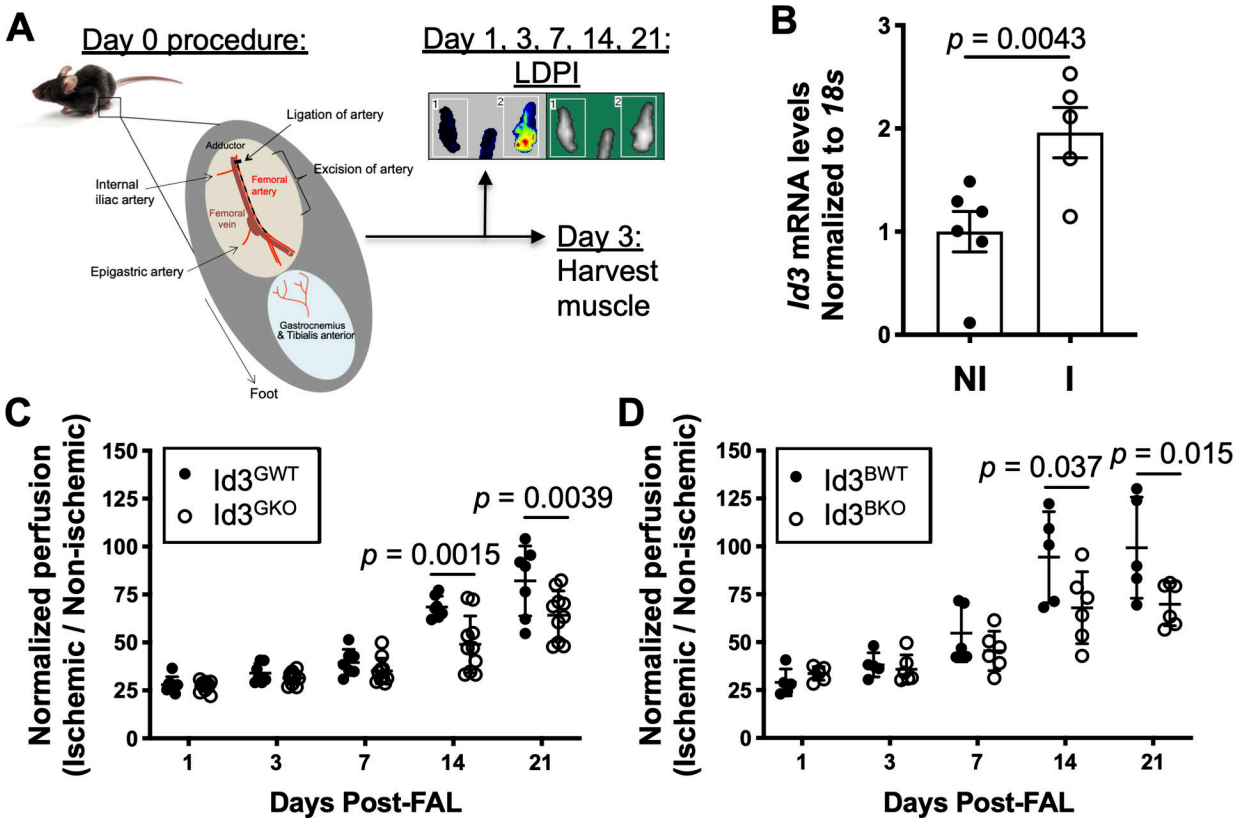

Figure 1. Id3 regulates blood flow in a B cell-specific manner.

(A) Schematic of the murine model of hind limb ischemia (HLI) and quantification of microvascular blood flow using laser Doppler perfusion imaging. (B) mRNA levels of *Id3* in ischemic (I) and non-ischemic (NI) gastrocnemius muscle lysates at day 3 of HLI. (C) Results from laser Doppler perfusion imaging (LDPI) quantifying blood flow in the feet of $Id3^{GWT}$ and $Id3^{GKO}$ littermate males at days 1, 3, 7, 14, and 21 days post-femoral artery ligation. Blood flow is quantified as the proportion of blood flow in the I foot over blood flow in the NI foot per mouse. (D) Blood flow results in $Id3^{BWT}$ and $Id3^{BKO}$ male littermates. Data shown is the mean ± SD. Statistical analyses were performed using Mann Whitney test (B) and two-way ANOVA (C,D).

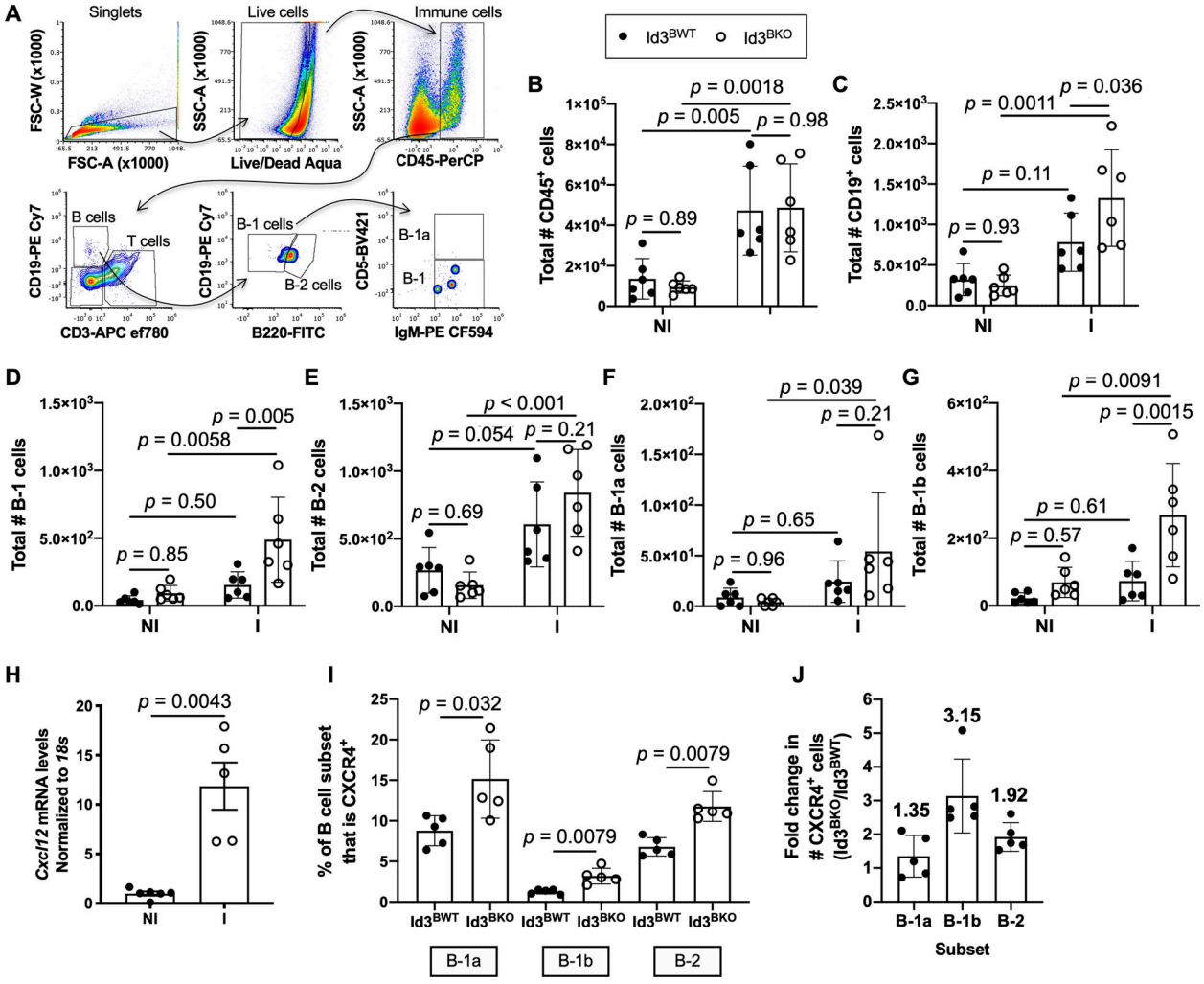

Figure 2. Loss of Id3 in B cells results in increased B-1b cell numbers in ischemic skeletal muscle.

(A) Flow cytometry gating strategy for identifying immune cell populations in digested gastrocnemius muscles at day 7 of HLI. (B-G) Total $CD45^+$ cells (B), total $CD19^+$ B cells (C), total $CD19^+B220^{low}$ B-1 cells (D), total $CD19^+B220^{high}$ B-2 cells (E), total $CD5^+$ B-1a (F), and total $CD5^-$ B-1b cells (G) per gastrocnemius muscle were quantified. (H) mRNA levels of *Cxcl12* in NI and I gastrocnemius muscle lysates at day 3 of HLI. (I) Proportion of peritoneal cavity B-1a, B-1b, and B-2 cells that are CXCR4+ at day 7 of HLI. (J) The number of peritoneal cavity $Id3^{BKO}$ $CXCR4^+$ B-1a, B-1b, and B-2 cells normalized to $Id3^{BWT}$ $CXCR4^+$ B cell subset numbers. Data shown is the mean ± SD. Statistical analyses were performed using two-way ANOVA (B-G) and Mann Whitney tests (H, I).

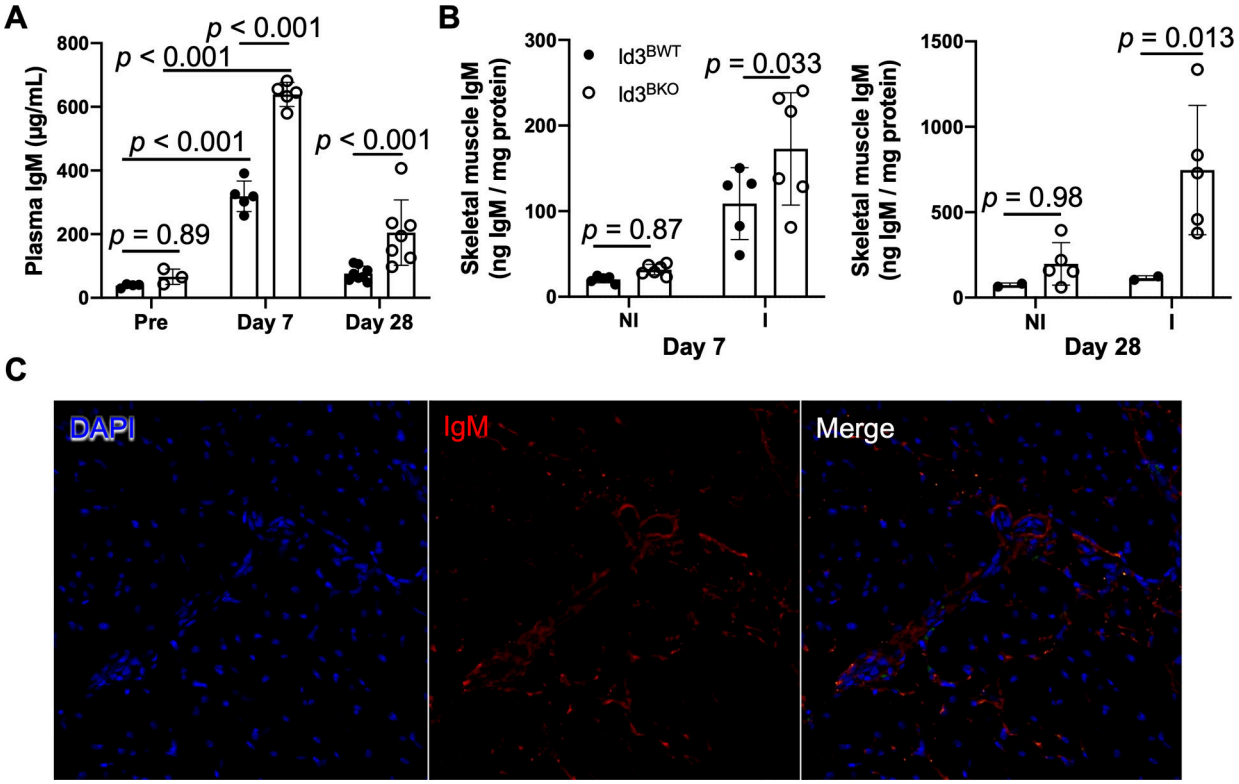

Figure 3. Id3^{BKO} mice have increased circulating and local levels of IgM.

(A) Total IgM in plasma from Id3^{BWT} and Id3^{BKO} mice was measured by ELISA at pre-HLI, Day 7, and Day 28 of HLI. (B) Total IgM levels in NI and I skeletal muscle at days 7 and 28 of HLI were measured by ELISA. (C) IgM and DAPI staining in ischemic gastrocnemius muscle from day 21 of HLI. Data shown is the mean ± SD. Statistical analyses were performed using two-way ANOVA.

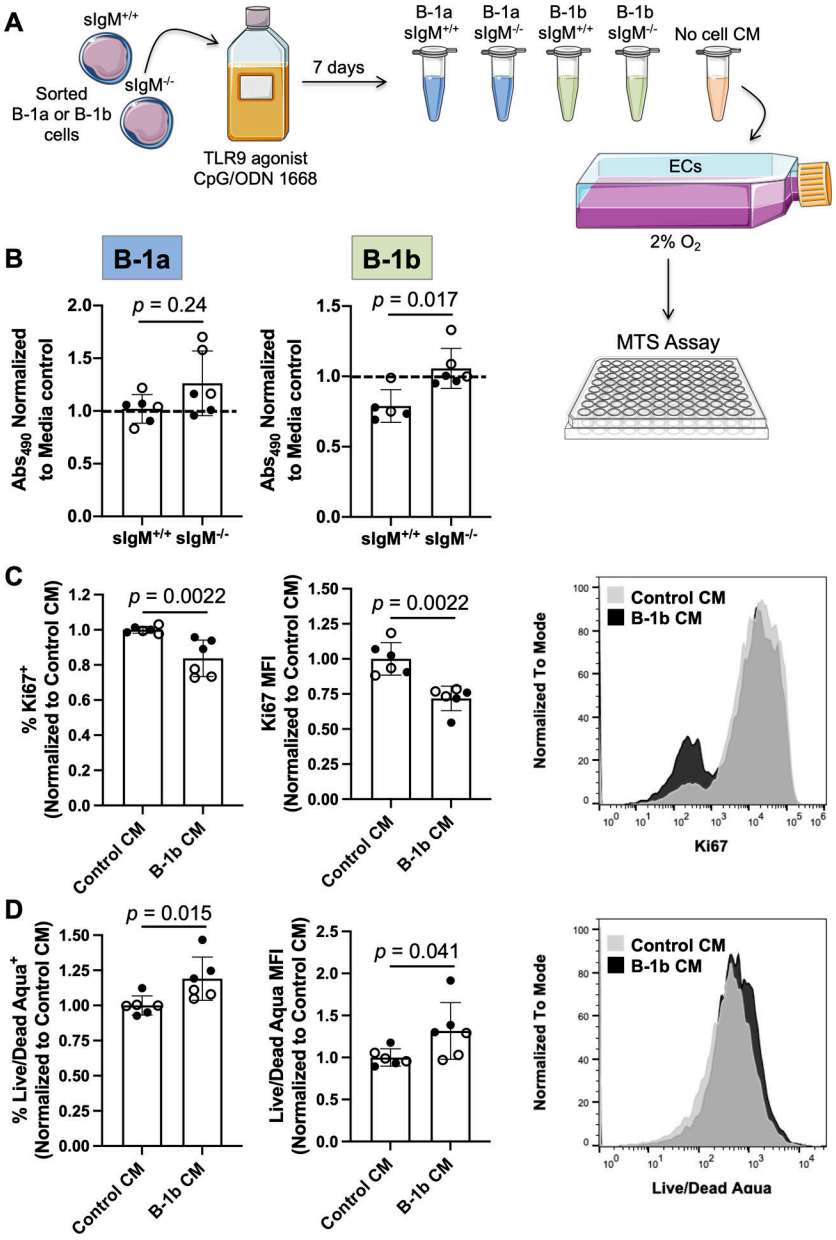

Figure 4. B-1b-produced IgM inhibits EC proliferation and survival *in vitro*.

(A) B-1b and B-1a cells from sIgM$^{+/+}$ and sIgM$^{-/-}$ mice were sorted by flow and stimulated *in vitro* by a TLR9 agonist CpG/ODN 1668 for 7 days to induce IgM production. The conditioned media (CM) from each stimulation was then used to treat ECs in the setting of hypoxia (2% O_2). To account for affects induced by TLR9 agonist remaining in the CM, this agonist was included in the vehicle control. Cell numbers following 24 hours of culture in hypoxia were quantified by MTS assay and normalized to media-only controls. (B) HUVEC numbers after treatment with B-1a CM and B-1b CM were measured. (C,D) Murine EC proliferation (C) and cell death (D) was quantified using flow cytometry. Data points from each independent experiment are represented by different symbols. Data shown is the mean ± SD. Statistical analyses were performed using Mann Whitney tests.

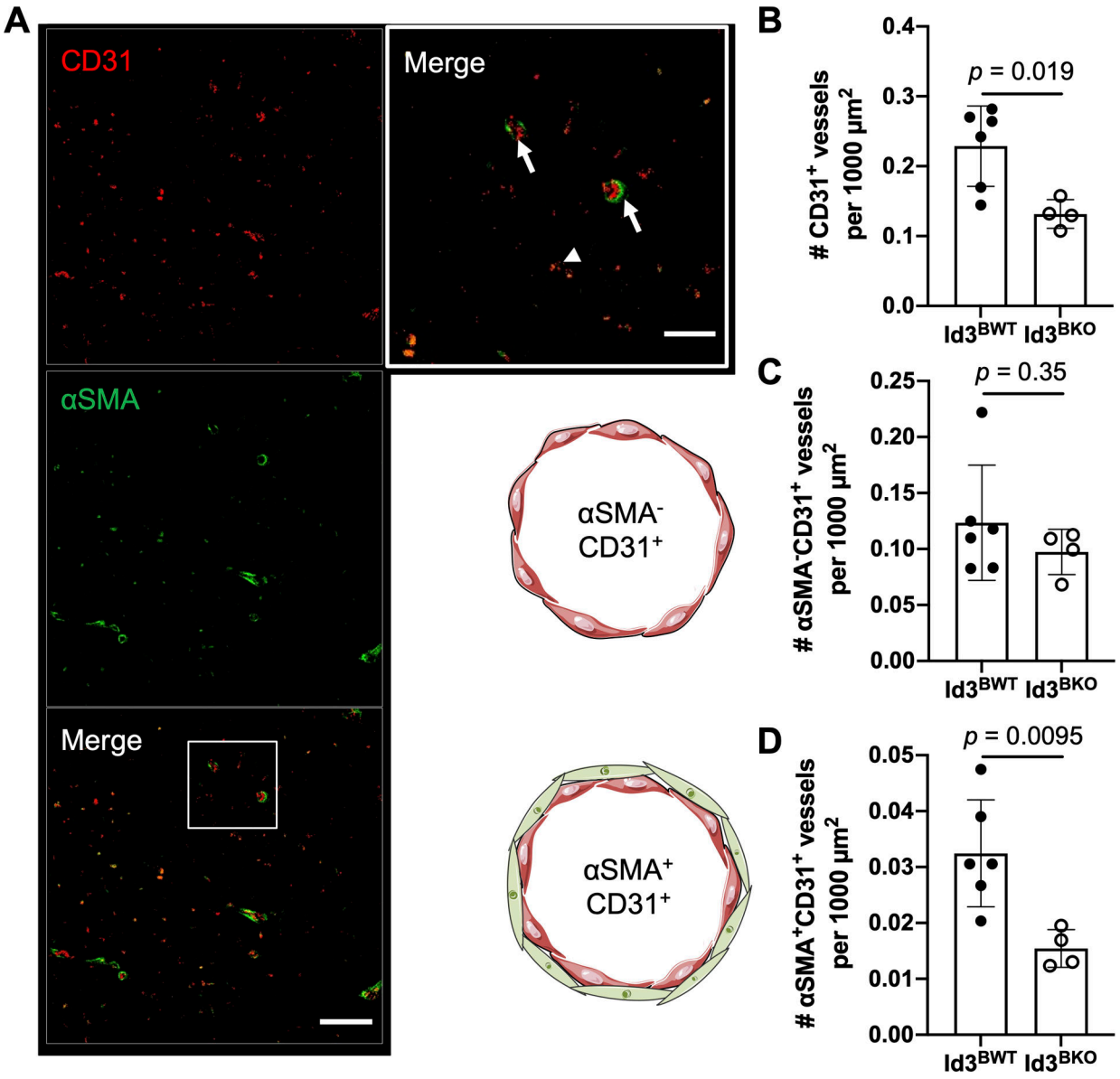

Figure 5. Id3^{BKO} mice have reduced vascular density in ischemic tibialis anterior muscles.

(A-D) Ischemic tibialis anterior (TA) muscles from Id3^{BWT} and Id3^{BKO} mice were harvested at day 28 of HLI, then fixed, embedded, and sectioned. Sections were stained with antibodies against EC marker CD31 and contractile protein αSMA, which is typically expressed in perivascular cells such as pericytes and VSMCs. (A) A representative image of CD31^{+} and αSMA^{+} is provided. The white arrows point to αSMA^{+}CD31^{+} structures, or vessels, while the arrowhead points to a αSMA^{-}CD31^{+} structure, or vessel. Scale bar delineates 50 μm in the left-hand Merge panel. The righthand Merge panel shows a higher magnification of both specified structures and the scale bar delineates 25 μm. (B-D) The number of total CD31^{+} vessels (B), CD31^{+}αSMA^{-} capillaries (C), and αSMA^{+}CD31^{+} vessels (D) per muscle section were averaged across sections per mouse. Data shown is the mean ± SD. Statistical analyses were performed using Mann Whitney tests.